Research Article | Vol. 31, No. 13 / 19 Jun 2023 / Optics Express 21482
Optics EXPRESS

High-resolution mid-infrared spectroscopy based on ultrafast Cr:ZnSe laser

EDOARDO VICENTINI,[1,2] ALESSIO GAMBETTA,[2,3] FRANCESCO CANELLA,[2,3] NICOLA COLUCCELLI,[2,3] PAOLO LAPORTA,[2,3] AND GIANLUCA GALZERANO[2,*]

[1]CIC nanoGUNE, Basque Research and Technology Alliance, Tolosa Hiribidea, 76 Donostia-San Sebastián, 20018, Spain
[2]Istituto di Fotonica e Nanotecnologie, Consiglio Nazionale delle Ricerche, Piazza Leonardo Da Vinci, 32, Milan 20133, Italy
[3]Dipartimento di Fisica, Politecnico di Milano, Piazza Leonardo Da Vinci, 32, Milano 20133, Italy
*gianluca.galzerano@cnr.it

Abstract: High-resolution broadband direct frequency comb spectroscopy in the mid-infrared spectral region is an extremely powerful and versatile experimental technique that allows study of the molecular structure of gaseous compounds with multiple applicative and scientific implications. Here we present the first implementation of an ultrafast Cr:ZnSe mode-locked laser covering more than 7 THz at around the emission wavelength of 2.4 μm, for direct frequency comb molecular spectroscopy with a frequency sampling of 220 MHz and a frequency resolution of ~100 kHz. This technique is based on a scanning micro-cavity resonator with a Finesse of ~12,000 and a diffraction reflecting grating. We demonstrate its application in high-precision spectroscopy of the acetylene molecule by retrieving line center frequencies of more than 68 roto-vibrational lines. Our technique paves the way for real time spectroscopic studies as well as for hyperspectral imaging techniques.

1. Introduction

Direct frequency-comb spectroscopy (DFCS) relies on a frequency-stabilised passive mode-locked laser coupled to a detection apparatus which enables real time detection of a broad portion of the source spectrum with extremely high spectral resolution, down to the frequency separation between the discrete spectral features (comb modes) of the source [1,2]. Thanks to its unique capabilities of combining high-speed and high-resolution with ultra-broadband and ultra-sensible detection DFCS has become an assessed and versatile tool in many areas of fundamental and applied science [3–6]. In the field of molecular spectroscopy and spectrometry for instance, DCFS allows not only for ultra-precise acquisition of broad molecular spectra [7,8] but also for real-time detection and identification with high sensitivity of trace amounts of molecules in gas phase even at remote distance [9,10] and with crowded mixtures [11].

The capability of resolving the single-comb mode is fundamental in precision spectroscopy applications where very narrow spectral features have to be detected over wide spectral bandwidths with absolute referencing of the optical frequency axis. An important requirement to be addressed in this particular field is also the capability of extending the optical bandwidth of operation to the mid-IR spectral region, to exploit the most intense molecular absorption features (fundamental transitions) lying in the so called "fingerprinting region" between ~ 2.5 μm and ~ 15 μm, allowing for a potential increase up to three orders of magnitude in the sensitivity with respect to the overtone transitions in the near-infrared (NIR). Several DFCS detection methods have been developed so far, with frequency resolution ranging from tens of kilohertz to a few-gigahertz level (depending on optical bandwidth and acquisition times) each one characterised by advantages and disadvantages in terms of complexity and cost-effectiveness. Moreover, some of these techniques

#491397 https://doi.org/10.1364/OE.491397
Journal © 2023 Received 22 Mar 2023; revised 18 May 2023; accepted 18 May 2023; published 12 Jun 2023

Optics EXPRESS

can be straightforwardly exploited in the mid-IR while others face several technological issues that limit this possibility at present. For example, dual-comb spectroscopy method, based on two comb sources with slightly detuned comb-line spacing [12], demonstrated excellent performance across a wide electromagnetic spectrum from visible to the far infrared [13–18] and feasible implementation also in the UV region [19,20] initially at the price of the use of two comb sources and the need of non-trivial stabilisation schemes to control the relative coherence between the two combs [21–24] which nowadays can be overcome by using a unique laser source emitting a dual comb coherent radiation [25,26]. Other DFCS methods demonstrating single-comb tooth detection, such as Fourier Transform InfraRed (FTIR) [27,28] Virtually Imaged Phased Array (VIPA) [29–31] and Vernier [7,32–34] spectroscopy techniques, suffers from some drawbacks in terms of complexity, measurement speed and spectral coverage. FTIRs for instance requires scanning arms equal to the speed of light divided by the comb mode spacing (30 cm for 1 GHz comb mode spacing), VIPA devices are not available in the whole fingerprinting spectral region while Vernier filtering relies on a precise syncronisation between the optical modes of the comb source and the transmission modes of the cavity.

In this paper, we present an alternative DFCS approach based on a high-finesse scanning micro-cavity resonator, SMART DFCS (Scanning Micro-cAvity ResonaTor DFCS) [35,36], in combination with an ultrafast Cr:ZnSe laser at around 2.4 μm. As already demonstrated in the NIR spectral region [35,36] this technique has the advantage of combining an architecture of much lower complexity with state-of-the-art performances in terms of frequency resolution and acquisition speed. Here, we show that this method can be effectively exploited in the mid-IR region enabling for a boost in sensitivity that comes form the access to the stronger molecular absorption lines lying in this spectral region.

2. Methods

The SMART approach shares with the Vernier spectroscopic method the adoption of a high-finesse optical cavity that act as a narrow-band filter which samples only few comb modes, very distant in frequency, so that a standard dispersive element (like a diffraction grating) is able to spatially separate them onto several detection elements (photodiode arrays, CCD pixels) for parallel acquisition (Fig. 1). A wide spectral separation FSR_v (free-spectral-range) between the filtered modes is achieved in the Vernier approach by exploiting the aliasing between two slightly different periodic functions, namely the comb mode spacing f_r and the cavity mode spacing $\Delta\nu_v$ which is slightly detuned from f_r by a small amount ϵ as shown in Fig. 2 (gray lines). In the following discussion the subscript "v" will always refer to parameters relative to the Vernier whereas the subscript "s" will be adopted for the smart technique. The SMART approach on the other hand exploits a Fabry-Perot cavity with a very small mirror separation d, of the order of $d \sim 100\mu$m, in such a way that a wide FSR_s is directly provided by the large mode separation $\Delta\nu_s \simeq FSR_s$ of the micro-cavity itself (fig. 2, blue lines), which results in the ~THz order of magnitude [35]. The full comb spectrum is recovered (in both schemes) by scanning the position of one of the cavity mirrors which results into a frequency-sweep of the transmission peaks of the cavity. The corresponding transmission signal vs time is then recorded by a photodiode as the convolution between the line-shape of each comb mode and the much broader spectral profile of the cavity modes.

The requirement of a fixed frequency relationship between f_r and $\Delta\nu_v$ makes the Vernier approach strongly dependent on the repetition rate of the comb source adopted and most important requires additional synchronisation electronic between laser and cavity compared to the SMART approach which in turn can be adapted to any source and allows to perform free running scans. Secondly the very short cavity length shortens by several orders of magnitude the photon lifetime allowing for faster acquisition [33]. Finally the compactness and robustness of the SMART detection system makes it a solid choice in the design of portable systems for field applications. A

Optics EXPRESS

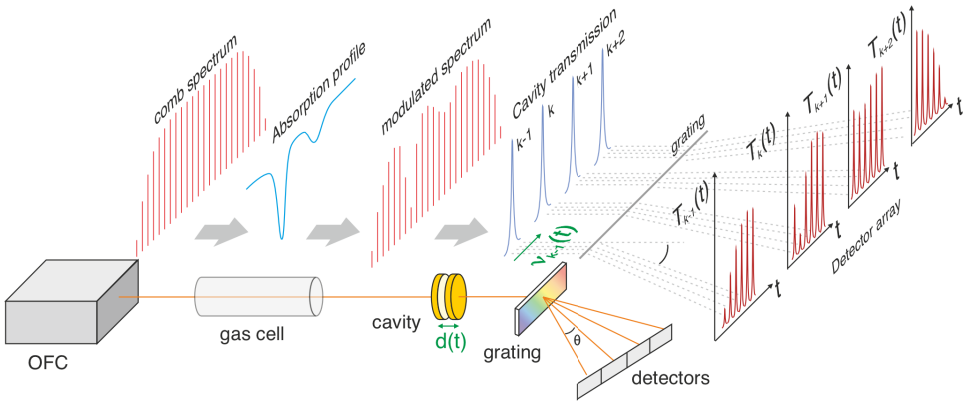

Fig. 1. Working principle of the SMART spectroscopic method: the spectrum of the ultrafast laser, constituted by a comb of equally spaced optical frequencies, is modulated by the absorption features of the molecular sample, then analyzed by a scanning optical cavity with a linewidth narrower than the comb spacing ($\delta\nu_s < f_r$). The microcavity transmission is further filtered by a low resolution diffraction grating and the single comb modes detected by several photo-detectors

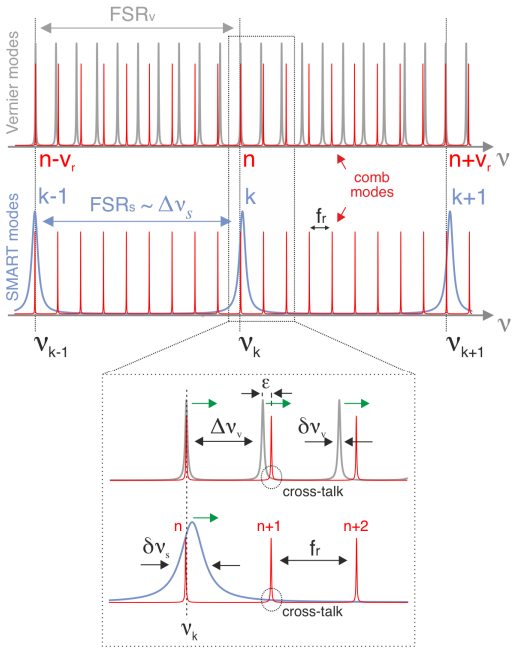

Fig. 2. Comparison between Vernier and SMART methods: the FSR_v of the Vernier measurement arises from the periodic coincidence between one of the cavity modes (in gray) and one of the comb modes (red) which takes place every ν_r cavity modes ($\nu_r = f_r/\epsilon$ being the Vernier-ratio of the system) at optical frquencies ν_{k-1}, ν_k, etc. A similar frequency separation between transmitted comb frequency is provided by the wide FSR_s of SMART cavity modes (blue). Green arrows indicate the scan direction of the cavity modes). Spectral crosstalk mechanism is evidenced for both techniques.

Optics EXPRESS

drawback shared by the two techniques is connected with the high-resolution filtering condition that must be fulfilled to achieve single comb-mode transmission with minimal crosstalk between adjacent comb modes. In case of Vernier filtering the required condition is for $\delta\nu_v$ to be much smaller than ϵ while for the SMART approach $\delta\nu_s$ must be smaller than the repetition rate f_r. In both cases a high cavity finesse over the whole comb spectrum must be ensured and this may not be easy in the mid-IR due to the lower availability of broadband high-reflection coatings with respect to the NIR spectral region. In the following section we demonstrate that nonetheless the SMART method performs very well also in the mid-IR, even with moderate finesse (~12,000) resonators where the above condition is somehow relaxed.

3. Experimental setup

The implementation of the SMART method in the spectral region from 2.3 μm to 2.5 μm is presented in Fig. 3. The mid-infrared ultrafast laser source is a Kerr-lens mode-locked Cr:ZnSe laser emitting 45-fs pulses at 2.4 μm with an average output power of 120 mW and a repetition rate of 220 MHz, phase-locked to a radio-frequency synthesizer [37]. The laser spectrum covers a FWHM bandwidth of ~135 nm corresponding to an emission range from 121.5 to 128.5 THz. The mid-IR radiation is coupled to the scanning microresonator through a 30-dB optical isolator and a mode-matching lens. The microresonator (a modified commercial interferometer) is constituted by two spherical mirrors (1 m of radius of curvature) spaced by ~300 μm, corresponding to a $\Delta\nu_s \simeq FSR_s$ of ~500 GHz (from now on we will refer to the SMART cavity mode-spacing with the generic acronym FSR). One of the two mirrors is mounted on a piezo-electric transducer which can scan the microresonator length up to 5 μm. The mirror movement is controlled by a periodic high voltage ramp which scan back and forward the mirror in 100 ms.

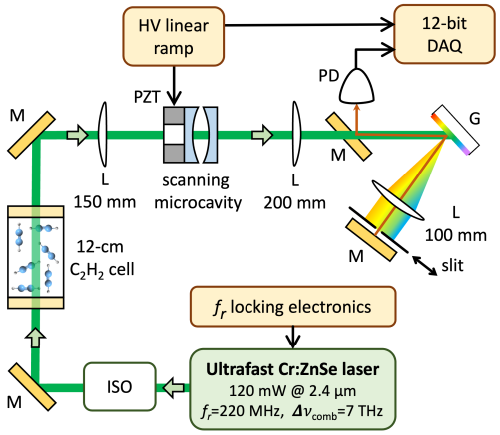

Fig. 3. Schematic representation of the SMART setup at 2.4 μm. DAQ: data acquisition board; G: diffraction grating; L: plano convex lens; M: mirror; ISO: optical isolator; PD: photodetector; PZT piezo electric transducer.

As previously mentioned, obtaining a high finesses can be challenging in the mid-IR region. The mirrors adopted in our setup have a nominal reflectivity of 99.994% at 2.3 μm which reduces to 99.992% at 2.4 μm and to 99.975% at 2.5 μm. This reflects into a change of the cavity finesse from a maximum value of ~52,000 to a minimum of ~12,000 across the spectrum of the Cr:ZnSe laser. At 2.44 μm the measured microresonator finesse is 12300, in quite good agreement with the nominal value (and four times lower than the value reported in previous experiments at around 1.55 μm [35,36]). To avoid spectral aliasing and resolve the single comb tooth, the microresonator transmission is filtered by a standard $4-f$ optical tunable filter (OTF)

Optics EXPRESS

consisting in a low dispersion reflecting grating (300 grooves/mm) followed by an adjustable slit and a back-reflecting plane mirror. After spectral filtering the light is focused onto a low-noise extended InGaAs detector with a bandwidth of 10 MHz. The detected signal is then acquired by a 12-bit oscilloscope, at a sampling frequency of 2.5 MSa/s.

To recover the full spectrum of the source we perform sequential acquisitions of contiguous spectral portions, selected by moving the slit along the spatially-dispersed comb spectrum. In practical applications where fast-detection may be required a photodiode array can be used instead, allowing for parallel acquisition of the whole comb spectrum in a single-scan.

The characterization of the SMART method has been carried on by performing direct absorption measurements of the acetylene ($^{12}C_2H_2$) molecule in gas form (99% purity) contained in a 12-cm long cell at an adjustable pressure. Acetylene presents intense vibrational transitions in the spectral region at around 2.44 μm (corresponding to 4100 cm^{-1}), belonging to the $\nu_1 + \nu_5^1$ inter-combination band of CH stretch and CH bending, with line intensities up to $6.6 \cdot 10^{-21}$ cm/molecule [38]. In particular, more than 68 rotovibrational lines of $^{12}C_2H_2$ belonging to the P, Q, and R branches of the $\nu_1 + \nu_5^1$ inter-combination band have been measured over an optical bandwidth from 2.41 to 2.49 μm (corresponding to a bandwidth of ~4 THz).

The absolute calibration of the frequency scale of the measured spectra has been retrieved by comparison with the HITRAN2020 database [39]. In particular, the strongest absorption line center frequency is assigned using the corresponding HITRAN value, while all the others points of the optical frequency axis are assigned by adding or subtracting a multiple of the comb spacing (i.e. the laser repetition frequency, which is phase locked to a GPS-disciplined Rb oscillator).

4. Results and discussion

In this first implementation of the SMART method in the mid-IR spectral region, we devoted particular attention to the characterisation of the spectrometer performance as a function of the microresonator linewidth $\delta\nu_{res}$. A critical condition which deserves careful investigation is reached in spectral regions where, due to the lower value of the finesse, $\delta\nu_{res}$ increases to values comparable to f_r: in this condition the line-shape of each transmitted comb mode become so broad that it starts to partially overlap with that related to neighbour modes, as shown in Fig. 4. This condition may in principle lead to a loss of frequency resolution and to a distortion of the measured absorption profiles due to signal cross-talk between neighbour comb modes.

In this regard, a comparison between two different microresonator linewidths, 35 and 98 MHz respectively, is shown in Fig. 4. The increase of the cavity linewidth is obtained by decreasing the cavity mirrors separation for the purpose of investigating the effect discussed above. In both cases, the frequency comb is probing the 12-cm long cell filled with C_2H_2 at a pressure of 50 mbar. Figures 4(a) and (e) show the single scan acquired over ~70 ms and corresponding to a cavity length tuning of ~1.2 μm. To retrieve the cavity single mode linewidth its transmission signal is de-convoluted with a series of equidistant modes with narrow linewidth (100 kHz) representing the frequency comb modes (as measured in [40]). Figures 4(c) and (g) report a detailed view of five adjacent comb modes together with the fitted profiles. From the retrieved linewidths we estimate two values of FSR_1 = 430 GHz and FSR_2 = 1200 GHz respectively for the two conditions and a corresponding finesse value of 12265 ± 20.

For an operational evaluation of how the cavity frequency resolution affects a real spectroscopic measurement, we compared the lineshape profiles between the several measured absorption spectra and the corresponding profiles computed using the HITRAN2020 database. As an example, Figs. 4(d) and (h) show the same C_2H_2 absorption line at 122.79 THz, $R1e$ transition belonging to the $\nu_1 + \nu_5^1$ vibrational band, measured with the two different cavity linewidths together with the computed line profile (Voigt profile) using HITRAN spectroscopic data. From the analysis of the residuals, it is worth noting that the main difference between the two measurements is related only to the signal-to-noise ratio (SNR), whereas the contribution

Optics EXPRESS

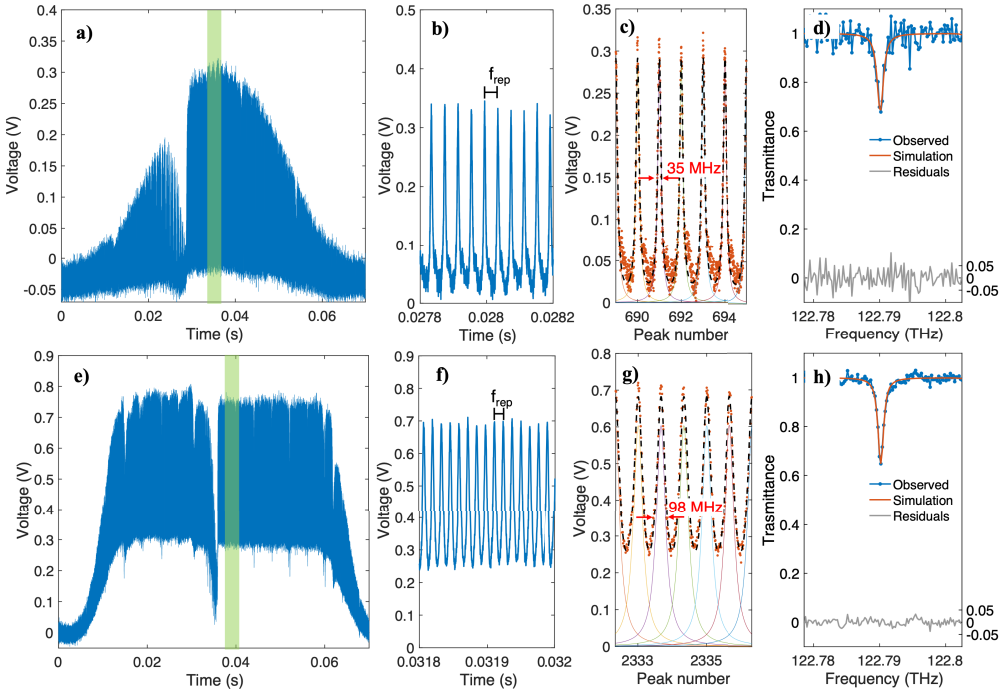

Fig. 4. SMART acquisition with two different micro cavity FSR, 430 GHz (a)-(d) and 1200 GHz (e)-(h). (a),(e) Acquired data as a function of time (the deep modulations of the acquired spectra are due to the C_2H_2 absorption lines). (b),(f) Zoom of panel (a),(e) in the green box. (c),(g) Fit of 5 frequency comb modes. Orange dots represent the acquired data; color solid lines represent single mode contribution to the fit. (d),(h) Measured C_2H_2 $R1e$ transmission profile blue line and best fit orange line with on the bottom the residuals.

of the microresonator linewidth does not significantly distort the measured line profiles (flat residuals). The effect of the microresonator instrumental response on the distortion of the measured spectroscopic features is evaluated by a numerical computation of the convolution integral between the comb spectrum and the microresonator line profile. For the $R1e$ transition reported in Figs. 4(d) and (h), this effect translates in uncertainty on the measured parameter (like line intensity or pressure) respectively of 0.7% and 5%, consistent with the available SNR and with the limited experimental conditions (220 MHz comb mode separation and 300 MHz C_2H_2 linewidths).

The $R1e$ transition is also used to calculate the figure of merit (M) of the spectrometer, representing the time-averaged noise-equivalent absorption per spectral element [33] $M = \alpha_{min}\sqrt{T/N}$ where $\alpha_{min} = (SNR \cdot L)^{-1}$ is the minimum detectable absorption (L being the length of the gas cell), N is the number of comb modes measured in a scanning time T and SNR is calculated as the standard deviation of the difference between the acquired point and the best fit absorption profile. For the two configurations reported in Figs. 4 the computed figure of merits per spectral element are $M_1 = 9.97 \cdot 10^{-6}$ cm^{-1}Hz$^{-1/2}$ and $M_2 = 1.81 \cdot 10^{-6}$ cm^{-1}Hz$^{-1/2}$, respectively for the FSR_1 and FSR_2 conditions. This values could be improved by more than two orders of magnitude by exploiting a multi-pass cell to increase the absorption-path length, reaching values of M very close to the $M_{NIR} = 2.7 \cdot 10^{-9}$ cm^{-1}Hz$^{-1/2}$ that we obtained in the NIR region by exploiting an Er:fiber comb source combined with a 33 m optical-length Herriott cell [35]. Regarding the SNR, the main source of noise comes from the detector and laser intensity noise. The amplified InGaAs detector has a noise equivalent power of $\sim 3 \cdot 10^{-12}$ W/Hz$^{-1/2}$,

Optics EXPRESS

corresponding to a minimum detectable power of 9 nW over 10 MHz bandwidth, whereas the laser intensity noise is characterized by a relative fluctuations of 0.3% over an integration bandwidth from 10 Hz to 10 MHz [37]. Taking into account a comb power per mode on the detector of ~ 450 nW, considering a 75% transmission of the diffraction grating and a 20% transmission of the FP cavity, which operates at atmospheric pressure, the single scan SNR_1 is limited to ~50, in good agreement with the data reported in Fig. 4(d). At this level the laser relative intensity noise does not contribute significantly to the degradation of SNR. In the case of *FSR* equal to 1200 GHz, Fig. 4(h), the improvement to *SNR* = ~165 is mainly ascribable to the higher intensity transmitted by the cavity in correspondence to each comb mode due to the leakage contribution of adjacent modes.

To fully characterize the performance of the SMART method detailed spectroscopic investigations of the $\nu_1 + \nu_5^1$ vibrational band of $^{12}C_2H_2$ in the spectral region from 120 to 125 THz (from 2.4 to 2.5 μm) have been carried out. Figure 5(a) shows the Q-branch of $\nu_1 + \nu_5^1$ band at around 122.63 THz recorded at three different $^{12}C_2H_2$ pressure: 10, 40, and 100 mbar. Each single-scan measurement has been recorded in 100-ms time with a microcavity FSR of ~600 GHz. All the 29 rotovibrational transitions of the Q-branch are clearly resolved even at around 122.65 THz where the separation between lines is lower than 1 GHz and the Doppler-broadened full-width at half-maximum is 295 MHz. Each transmission profile has been fitted using the spectroscopic parameters reported in HITRAN2020 database, such as line strength, pressure broadening, and pressure shift coefficients. Figure 5(b) reports the measured transmission spectrum together with the best fitting profile for a nominal C_2H_2 pressure of 40 mbar. The root-mean-squared value of the fit residuals, 0.3%, corresponds to a SNR of ~ 150. It is worth noting that in Fig. 5(b) low C_2H_2 absorption features with line contrasts of 5.5% and 4.5% can be detected at 122.582 THz and 122.595 THz, respectively, although a fit residual peak to peak value of 2% is observed in this frequency range. In addition, from the fitting procedure it is also possible to retrieve a C_2H_2 pressure of 39.4 ± 1.8 mbar (being the contribution of the gas cell length uncertainty negligible with respect to the fit residuals), in very good agreement with the value measured by the gas-cell pressure gauge, characterized by an uncertainty of ±5 mbar in the range from 10 to 1000 mbar and by ±0.5 mbar in the range from 0.5 to 9.9 mbar. By repeating the measurements at different C_2H_2 pressure values in the range from 10 to 100 mbar, we were also able to compare the pressure values retrieved by the spectroscopic method with those measured by the pressure gauge, as shown in Fig. 5(c). The agreement between the two sets of data is rather good (inside the tolerance range of the pressure gauge), demonstrating the capability of SMART spectroscopy to precisely measure line profiles and retrieve either spectroscopic parameters or environmental parameters such as partial pressure and concentration.

To further test the frequency accuracy performance of the implemented spectroscopic method over the whole bandwidth covered by the ultrafast Cr:ZnSe laser, the measurement of the entire $\nu_1 + \nu_5^1$ vibrational band of the C_2H_2 is performed at a gas pressure of 50 mbar. Figure 6(a) reports the recorded transmission spectrum in the spectral region between 120 THz and 125 THz together with the fitted profile (HITRAN2020 database), showing the *P*, *Q* and *R* branches of the $\nu_1 + \nu_5^1$ band in combination with atmospheric water vapor absorption lines. These last are mainly due to the water vapor present inside the Cr:ZnSe laser cavity (no nitrogen purging) that strongly distorts the laser emission spectrum at around water vapour absorptions. These intracavity water absorptions do not produce a simple absorption feature but a more complex shape related to the complex refraction index of the absorber that can be modelled as a linear combination of real and imaginary part of the absorption profiles [41]. To cover the 5-THz optical bandwidth 8 single-scans (no averaging) with a microresonator FSR of 1 THz have been acquired by moving the adjustable slit of the 4-f filter to select a different portion of the spectrum at each measurement. Each frequency windows partially overlapped with the successive. In this way it is possible to continuously acquire all the spectrum and calibrating the frequency axis using only a single C_2H_2

Optics EXPRESS

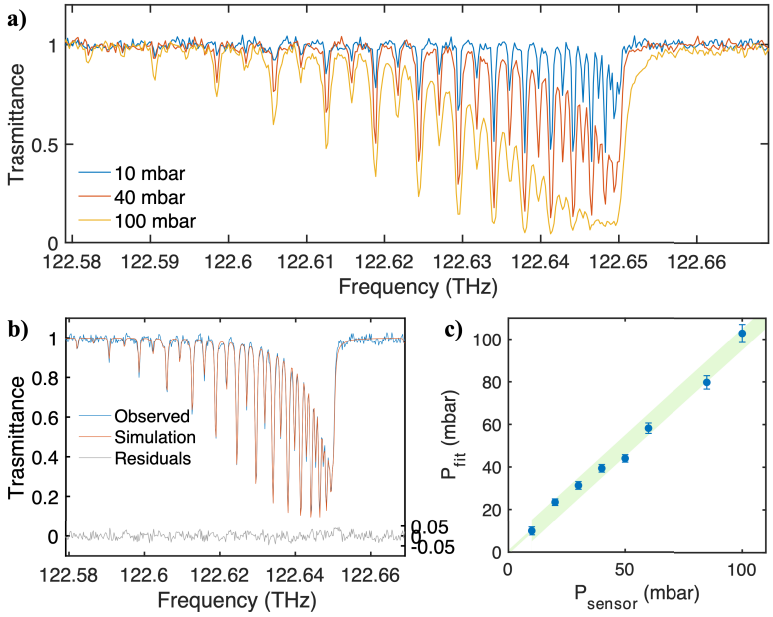

Fig. 5. (a) Measured acetylene transmission for three different pressures, 10 mbar blue, 40 mbar red, 100 mbar yellow. (b) Measured (blue), the best fit (orange) and the residuals (grey) of the transmission profile of acetylene at 40 mbar. (c) Best fit gas pressure vs pressure sensor measurement for acetylene gas between 10 mbar and 100 mbar. The best fit includes the errorbar of the fit corresponding to a 95% confidence interval. Green bands represent the ±5 mbar accuracy of the pressure gauge in the range 10-1000 mbar and ±0.5 mbar in the range 0.5-9.9 mbar.

absorption line. Each spectrum has been joined to the next by using C_2H_2 absorption lines which are in common between two successive windows, as reference points. The joined windows have been fitted all together and the obtained residuals are characterized by a standard deviation of 1.4% over 3.5 THz optical range. This larger deviation compared to those in Figs. 4 and 5 is due to the additional fitting parameters that must be computed to account the strong intracavity water absorptions. Figure 6(b) shows a zoom at around 121.85 THz corresponding to one of the overlapping regions between two adjacent frequency windows. No significant deviation (below 1%) between the recorded transmission spectra of the two windows are observed. The fit residuals show periodic structures due to the parasitic etalon effects of the absorption cell windows and of the antireflection coated lenses. For optical frequencies higher than 123 THz the parasitic etalon effects increase due to the higher value of the residual reflectivity of the gas cell windows. Figure 6(c) shows the deviation between the measured line center frequencies and the values reported in the HITRAN database (with a stated accuracy of 30 MHz). Each value is reported with its statistical uncertainty (2-σ value representing 95% of the confidence interval), which depends on the SNR of the recorded line profile. The root means squared value of the measured line center frequencies reported in Fig. 6(b) is 16 MHz representing the overall frequency accuracy of the implemented SMART method. This accuracy is limited not only by the SNR but also by the fact that the absolute calibration of the frequency axis is obtained from the HITRAN database (in the range 3-30 MHz for the most intense C_2H_2 lines) and not by the full self referecing of the ultrafast Cr laser. Indeed, in the present implementation, only the repetition frequency of the ultrafast Cr laser is referred to a RF standard while its carrier envelope offset (CEO) frequency is in free-running without any direct monitoring of its value. Assuming

Optics EXPRESS

a measurement time of few seconds for the acquisition of the full spectrum reported in Fig. 6, the contribution of the CEO frequency drift is in the 1-MHz range and therefore the HITRAN database mainly set the frequency accuracy. If better accuracies are desired, a self-referenced ultrafast Cr laser comb has to be used at the cost of increasing the experimental complexity of the spectroscopic tool.

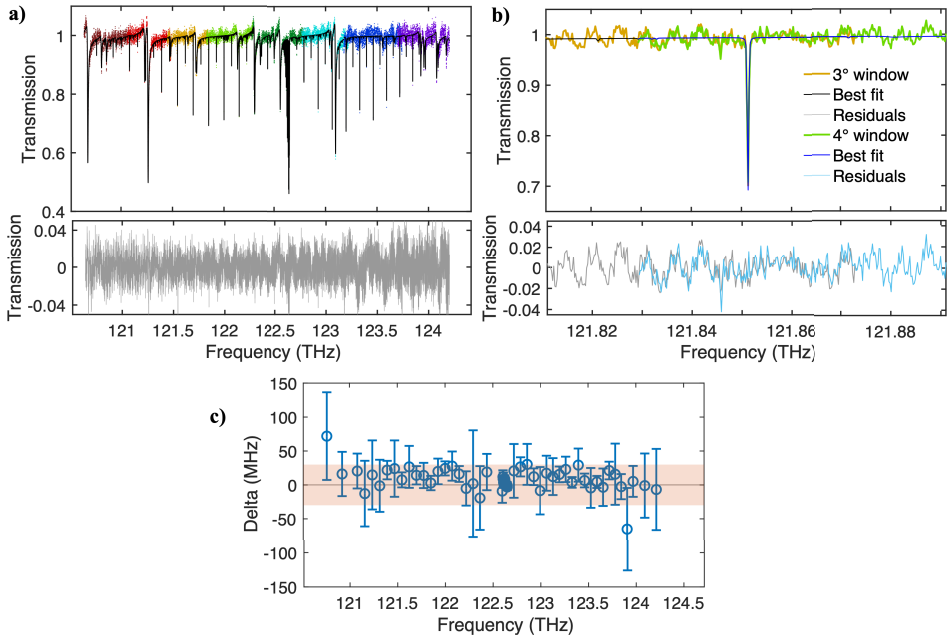

Fig. 6. (a) Transmission profile of acetylene at 10 mbar pressure, measured in 8 frequency windows (one for each color), with their best fit (black solid line) and the fit residual (grey solid line). (b) Detailed zoom of panel (a) showing the overlapping between two frequency windows. (c) Frequency difference between fitted line center (blue points) and HITRAN 2020 database. Each point is represented together with the fitting error bar representing the 95% confidence interval. The red region represents the upper limit of line center uncertainty of HITRAN 2020 for the represented absorption lines (30 MHz).

5. Conclusion

In conclusion, by exploiting a scanning micro-cavity Fabry-Perot resonator coupled to a Kerr-lens mode-locked Cr:ZnSe laser we were able to perform broadband precision-spectroscopy measurements in the mid-IR region around 2.4 μm by detecting several absorption lines of the $\nu_1 + \nu_5^1$ vibrational band of C_2H_2 inside a 12-cm long gas cell. We evaluated the SMART DFCS approach in this spectral region both in terms of sensitivity and resolution, in both cases obtaining values in line with our previous results in the NIR region. Regarding the measurement resolution, single comb-mode detection was achieved enabling the possibility of sub-MHz spectral resolutions [36] as well as sensitive pressure-dependent spectroscopic measurements over broad bandwidths as shown on the roto-vibrational absorption lines of the C_2H_2 Q-branch under several pressure conditions. With respect to the system sensitivity a minimum noise-equivalent-absorption per comb mode of $M = 1.81 \cdot 10^{-6}$ cm^{-1} Hz$^{-1/2}$ was obtained, limited mainly by the following factors: 1) low power per comb mode of the laser source with respect to the detector noise-equivalent-power, 2) short absorption-path due to the short length of the exploited gas-cell, 3) small bandwith acquired in a single scan due to the

Optics EXPRESS

employment of an OTF instead of a parallel detection of the whole laser bandwidth by means of a photodiode array. All these contributions, as previously discussed, can be easily overcome allowing for an improvement of M by several orders of magnitude, such as using commercially available amplified Cr:ZnS laser system to increase by more than one order of magnitude the comb mode power, multipass absorption cell to enhance path length by more than two orders of magnitude, and linear detector array to broad the optical bandwidth up to one order of magnitude. Finally it is worth to mention that in addition to the excellent performances reported in terms of bandwidth, resolution, sensitivity and acquisition speed the SMART approach greatly reduces the overall complexity of the system with a special regard to application-oriented designs. By adding an auxiliary CW reference laser with frequency stability better than the Cr:ZnSe pulse repetition frequency, also the absolute calibration of the frequency axis can be obtained without the need to use HITRAN database [35].

Funding. Ministero dell'Università e della Ricerca (IR0000016 - CUP B53C22001750006).

Acknowledgments. The authors acknowledge financial support by the European Union's NextGenerationEU Programme with the I-PHOQS Infrastructure [IR0000016, ID D2B8D520, CUP B53C22001750006] "Integrated infrastructure initiative in Photonic and Quantum Sciences."

Disclosures. The authors declare no conflicts of interest.

Data availability. Data underlying the results presented in this paper are not publicly available at this time but may be obtained from the authors upon reasonable request.

References

1. T. Udem, R. Holzwarth, and T. W. Hänsch, "Optical frequency metrology," Nature **416**(6877), 233–237 (2002).
2. D. J. Jones, S. A. Diddams, J. K. Ranka, A. Stentz, R. S. Windeler, J. L. Hall, and S. T. Cundiff, "Carrier-envelope phase control of femtosecond mode-locked lasers and direct optical frequency synthesis," Science **288**(5466), 635–639 (2000).
3. N. Picqué and T. W. Hänsch, "Frequency comb spectroscopy," Nat. Photonics **13**(3), 146–157 (2019).
4. S. A. Diddams, "The evolving optical frequency comb," J. Opt. Soc. Am. B **27**(11), B51–B62 (2010).
5. T. Ideguchi, S. Holzner, B. Bernhardt, G. Guelachvili, N. Picqué, and T. W. Hänsch, "Coherent raman spectro-imaging with laser frequency combs," Nature **502**(7471), 355–358 (2013).
6. E. Vicentini, Z. Wang, K. Van Gasse, T. W. Hänsch, and N. Picqué, "Dual-comb hyperspectral digital holography," Nat. Photonics **15**(12), 890–894 (2021).
7. M. Siciliani de Cumis, R. Eramo, N. Coluccelli, G. Galzerano, P. Laporta, and P. Cancio Pastor, "Multiplexed direct-frequency-comb vernier spectroscopy of carbon dioxide $2\nu_1 + \nu_3$ ro-vibrational combination band," J. Chem. Phys. **148**(11), 114303 (2018).
8. S. A. Meek, A. Hipke, G. Guelachvili, T. W. Hänsch, and N. Picqué, "Doppler-free fourier transform spectroscopy," Opt. Lett. **43**(1), 162–165 (2018).
9. G. B. Rieker, F. R. Giorgetta, W. C. Swann, J. Kofler, A. M. Zolot, L. C. Sinclair, E. Baumann, C. Cromer, G. Petron, C. Sweeney, P. P. Tans, I. Coddington, and N. R. Newbury, "Frequency-comb-based remote sensing of greenhouse gases over kilometer air paths," Optica **1**(5), 290–298 (2014).
10. L. Nugent-Glandorf, F. R. Giorgetta, and S. A. Diddams, "Open-air, broad-bandwidth trace gas sensing with a mid-infrared optical frequency comb," Appl. Phys. B **119**(2), 327–338 (2015).
11. M. J. Thorpe, D. Balslev-Clausen, M. S. Kirchner, and J. Ye, "Cavity-enhanced optical frequency comb spectroscopy: application to human breath analysis," Opt. Express **16**(4), 2387–2397 (2008).
12. I. Coddington, W. C. Swann, and N. R. Newbury, "Coherent multiheterodyne spectroscopy using stabilized optical frequency combs," Phys. Rev. Lett. **100**(1), 013902 (2008).
13. T. Ideguchi, A. Poisson, G. Guelachvili, T. W. Hänsch, and N. Picqué, "Adaptive dual-comb spectroscopy in the green region," Opt. Lett. **37**(23), 4847–4849 (2012).
14. A. Schliesser, M. Brehm, F. Keilmann, and D. W. van der Weide, "Frequency-comb infrared spectrometer for rapid, remote chemical sensing," Opt. Express **13**(22), 9029–9038 (2005).
15. B. Bernhardt, E. Sorokin, P. Jacquet, R. Thon, T. Becker, I. T. Sorokina, N. Picqué, and T. W. Hänsch, "Mid-infrared dual-comb spectroscopy with 2.4 μm Cr^{2+}:ZnSe femtosecond lasers," Appl. Phys. B **100**(1), 3–8 (2010).
16. G. Ycas, F. R. Giorgetta, E. Baumann, I. Coddington, D. Herman, S. A. Diddams, and N. R. Newbury, "High-coherence mid-infrared dual-comb spectroscopy spanning 2.6 to 5.2 μm," Nat. Photonics **12**(4), 202–208 (2018).
17. M. Yan, P.-L. Luo, K. Iwakuni, G. Millot, T. W. Hänsch, and N. Picqué, "Mid-infrared dual-comb spectroscopy with electro-optic modulators," Light: Sci. Appl. **6**(10), e17076 (2017).
18. I. Coddington, N. Newbury, and W. Swann, "Dual-comb spectroscopy," Optica **3**(4), 414–426 (2016).
19. V. Schuster, C. Liu, R. Klas, P. Dominguez, J. Rothhardt, J. Limpert, and B. Bernhardt, "Ultraviolet dual comb spectroscopy: a roadmap," Opt. Express **29**(14), 21859–21875 (2021).

Optics EXPRESS

20. S. Galtier, C. Pivard, and P. Rairoux, "Towards dcs in the uv spectral range for remote sensing of atmospheric trace gases," Remote Sens. **12**(20), 3444 (2020).
21. J. Roy, J.-D. Deschênes, S. Potvin, and J. Genest, "Continuous real-time correction and averaging for frequency comb interferometry," Opt. Express **20**(20), 21932–21939 (2012).
22. M. Cassinerio, A. Gambetta, N. Coluccelli, P. Laporta, and G. Galzerano, "Absolute dual-comb spectroscopy at 1.55 μm by free-running er:fiber lasers," Appl. Phys. Lett. **104**(23), 231102 (2014).
23. T. Ideguchi, A. Poisson, G. Guelachvili, N. Picqué, and T. W. Hänsch, "Adaptive real-time dual-comb spectroscopy," Nat. Commun. **5**(1), 3375 (2014).
24. G. Millot, S. Pitois, M. Yan, T. Hovhannisyan, A. Bendahmane, T. W. Hänsch, and N. Picqué, "Frequency-agile dual-comb spectroscopy," Nat. Photonics **10**(1), 27–30 (2016).
25. B. Willenberg, J. Pupeikis, L. M. Krüger, F. Koch, C. R. Phillips, and U. Keller, "Femtosecond dual-comb Yb_2CaF_2 laser from a single free-running polarization-multiplexed cavity for optical sampling applications," Opt. Express **28**(20), 30275–30288 (2020).
26. M. Kowalczyk, L. Sterczewski, X. Zhang, V. Petrov, Z. Wang, and J. Sotor, "Dual-comb femtosecond solid-state laser with inherent polarization-multiplexing," Laser Photonics Rev. **15**(8), 2000441 (2021).
27. P. Balling, P. Masika, K. Petr, and M. Dolezal, "Length and refractive index measurement by fourier transform interferometry and frequency comb spectroscopy," Meas. Sci. Technol. **23**(9), 094001 (2012).
28. P. Masłowski, K. F. Lee, A. C. Johansson, A. Khodabakhsh, G. Kowzan, L. Rutkowski, A. A. Mills, C. Mohr, J. Jiang, M. E. Fermann, and A. Foltynowicz, "Surpassing the path-limited resolution of fourier-transform spectrometry with frequency combs," Phys. Rev. A **93**(2), 021802 (2016).
29. S. A. Diddams, L. Hollberg, and V. Mbele, "Molecular fingerprinting with the resolved modes of a femtosecond laser frequency comb," Nature **445**(7128), 627–630 (2007).
30. L. Nugent-Glandorf, T. Neely, F. Adler, A. J. Fleisher, K. C. Cossel, B. Bjork, T. Dinneen, J. Ye, and S. A. Diddams, "Mid-infrared virtually imaged phased array spectrometer for rapid and broadband trace gas detection," Opt. Lett. **37**(15), 3285–3287 (2012).
31. G. Kowzan, D. Charczun, A. Cygan, R. S. Trawiński, D. Lisak, and P. Maslowski, "Broadband optical cavity mode measurements at hz-level precision with a comb-based vipa spectrometer," Sci. Rep. **9**(1), 8206 (2019).
32. C. Gohle, B. Stein, A. Schliesser, T. Udem, and T. W. Hänsch, "Frequency comb vernier spectroscopy for broadband, high-resolution, high-sensitivity absorption and dispersion spectra," Phys. Rev. Lett. **99**(26), 263902 (2007).
33. L. Rutkowski and J. Morville, "Broadband cavity-enhanced molecular spectra from vernier filtering of a complete frequency comb," Opt. Lett. **39**(23), 6664–6667 (2014).
34. C. Lu, J. Morville, L. Rutkowski, F. S. Vieira, and A. Foltynowicz, "Cavity-enhanced frequency comb vernier spectroscopy," Photonics **9**(4), 222 (2022).
35. A. Gambetta, M. Cassinerio, D. Gatti, P. Laporta, and G. Galzerano, "Scanning micro-resonator direct-comb absolute spectroscopy," Sci. Rep. **6**(1), 35541 (2016).
36. E. Vicentini, A. Gambetta, N. Coluccelli, Y. Wang, P. Laporta, and G. Galzerano, "Direct-frequency-comb spectroscopy by a scanning fabry-pérot microcavity resonator," Phys. Rev. A **102**(3), 033510 (2020).
37. Y. Wang, T. T. Fernandez, N. Coluccelli, A. Gambetta, P. Laporta, and G. Galzerano, "47-fs kerr-lens mode-locked cr:znse laser with high spectral purity," Opt. Express **25**(21), 25193–25200 (2017).
38. L. Rothman, D. Jacquemart, and A. Barbe, *et al.*, "The hitran 2004 molecular spectroscopic database," J. Quant. Spectrosc. Radiat. Transfer **96**(2), 139–204 (2005).
39. I. Gordon, L. Rothman, and R. Hargreaves, *et al.*, "The hitran2020 molecular spectroscopic database," J. Quant. Spectrosc. Radiat. Transfer **277**, 107949 (2022).
40. S. O. Leonov, Y. Wang, V. S. Shiryaev, G. E. Snopatin, B. S. Stepanov, V. G. Plotnichenko, E. Vicentini, A. Gambetta, N. Coluccelli, C. Svelto, P. Laporta, and G. Galzerano, "Coherent mid-infrared supercontinuum generation in tapered suspended-core $As_{39}Se_{61}$ fibers pumped by a few-optical-cycle cr:znse laser," Opt. Lett. **45**(6), 1346–1349 (2020).
41. V. L. Kalashnikov and E. Sorokin, "Soliton absorption spectroscopy," Phys. Rev. A **81**(3), 033840 (2010).